JACS
JOURNAL OF THE AMERICAN CHEMICAL SOCIETY

ARTICLE

pubs.acs.org/JACS

The Unique Alzheimer's β-Amyloid Triangular Fibril Has a Cavity along the Fibril Axis under Physiological Conditions

Yifat Miller,[†] Buyong Ma,[*,‡] and Ruth Nussinov[*,‡,§]

[†]Center for Cancer Research Nanobiology Program NCI-Frederick, Frederick, Maryland 21702, United States

[‡]Basic Science Program, SAIC-Frederick, Inc., Center for Cancer Research Nanobiology Program NCI-Frederick, Frederick, Maryland 21702, United States

[§]Sackler Institute of Molecular Medicine, Department of Human Genetics and Molecular Medicine, Sackler School of Medicine, Tel Aviv University, Tel Aviv 69978, Israel

Supporting Information

ABSTRACT: Elucidating the structure of Aβ_{1-40} fibrils is of interest in Alzheimer's disease research because it is required for designing therapeutics that target Aβ_{1-40} fibril formation at an early stage of the disease. M35 is a crucial residue because of its potential oxidation and its strong interactions across β-strands and across β-sheets in Aβ fibrils. Experimentally, data for the three-fold symmetry structure of the Aβ_{9-40} fibril suggest formation of tight hydrophobic core through M35 interactions across the fibril axis and strong I31−V39 interactions between different cross-β units. Herein, on the basis of experimental data, we probe conformers with three-fold symmetry of the full-length Aβ_{1-40}. Our all-atom molecular dynamics simulations in explicit solvent of conformers based on the ssNMR data reproduced experimental observations of M35−M35 and I31−V39 distances. Our interpretation of the experimental data suggests that the observed ~5−7 Å M35−M35 distance in the fibril three-fold symmetry structure is likely to relate to M35 interactions along the fibril axis, rather than across the fibril axis, since our measured M35−M35 distances across the fibril axis are consistently above 15 Å. Consequently, we revealed that the unique Aβ_{1-40} triangular structure has a large cavity along the fibril axis and that the N-termini can assist in the stabilization of the fibril by interacting with the U-turn domains or with the C-termini domains. Our findings, together with the recent cyroEM characterization of the hollow core in Aβ_{1-42} fibrils, point to the relevance of a cavity in A$\beta_{1-40/1-42}$ oligomers which should be considered when targeting oligomer toxicity.

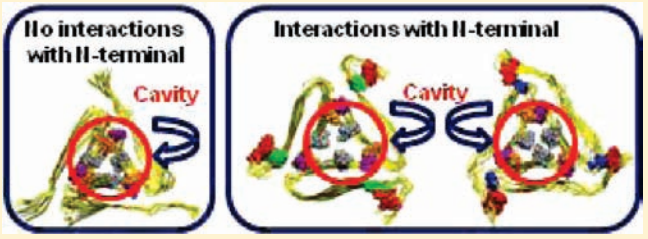

1. INTRODUCTION

Alzheimer's disease (AD) is the most common cause of dementia. Biochemical analysis revealed that the main constituent is a small polypeptide Aβ_{1-40} or Aβ_{1-42}, which is derived from endoproteolytic cleavage of the transmembrane amyloid precursor protein (APP).[1] While Aβ_{1-42} increases significantly in the brain,[2] Aβ_{1-40} is the most abundant Aβ isoform.[3] Peptide assembly from soluble oligomers into insoluble fibrils was suggested to occur via a multistep process;[4,5] however, this suggestion has been controversial. Full Aβ_{1-40} molecular structures are of interest in drug discovery which targets fibril formation at an early disease stage. ssNMR studies of Aβ_{1-40} fibrils led to two models: two-fold-symmetric[6] and three-fold-symmetric.[7] These reflect high population conformers under different experimental synthesis conditions. Both models exhibit in-register parallel twisted β-sheets constructed from nearly the same β-strand segments. In both models, the C-termini face the internal fibril surface and the N-termini are exposed to the exterior bulk solvent. They differ in non-β-strand segments (the U-turn and the flexible N-terminal domain) and in the quaternary structure (contacts between cross-β units). Based on ssNMR data of the full-length Aβ_{1-40} fibril,[7] the N terminal is less ordered and a molecular model for the three-fold symmetry is only available for Aβ_{9-40}.

In the two-fold-symmetric Aβ_{1-40}, M35 interactions along and across the fibril axis stabilize it. In the three-fold-symmetric Aβ_{1-40},[7] M35 residues also interact. If the interactions involve M35 from different β-sheets, it can be expected that no cavity will be formed in the core. We construct models that satisfy three-fold symmetry and compare them with ssNMR constraints.[7] We focus on two M35−M35 interaction types: along the fibril axis and across the cavity. While all interactions exhibit agreement with the experimental constraints, the M35−M35 interactions across a cavity disagree. Consequently, we suggest that the observed M35−M35 constraints are more likely to result from interactions along the fibril axis in the same sheet than across the fibril cavity.

2. MATERIALS AND METHODS

2.1. Experiment-Based Aβ_{1-40} Fibril Models Construction.

Herein, on the basis of Tycko's three-fold symmetry model,[7] we constructed

Received: November 16, 2010
Published: February 7, 2011

dx.doi.org/10.1021/ja1100273 | J. Am. Chem. Soc. 2011, 133, 2742–2748

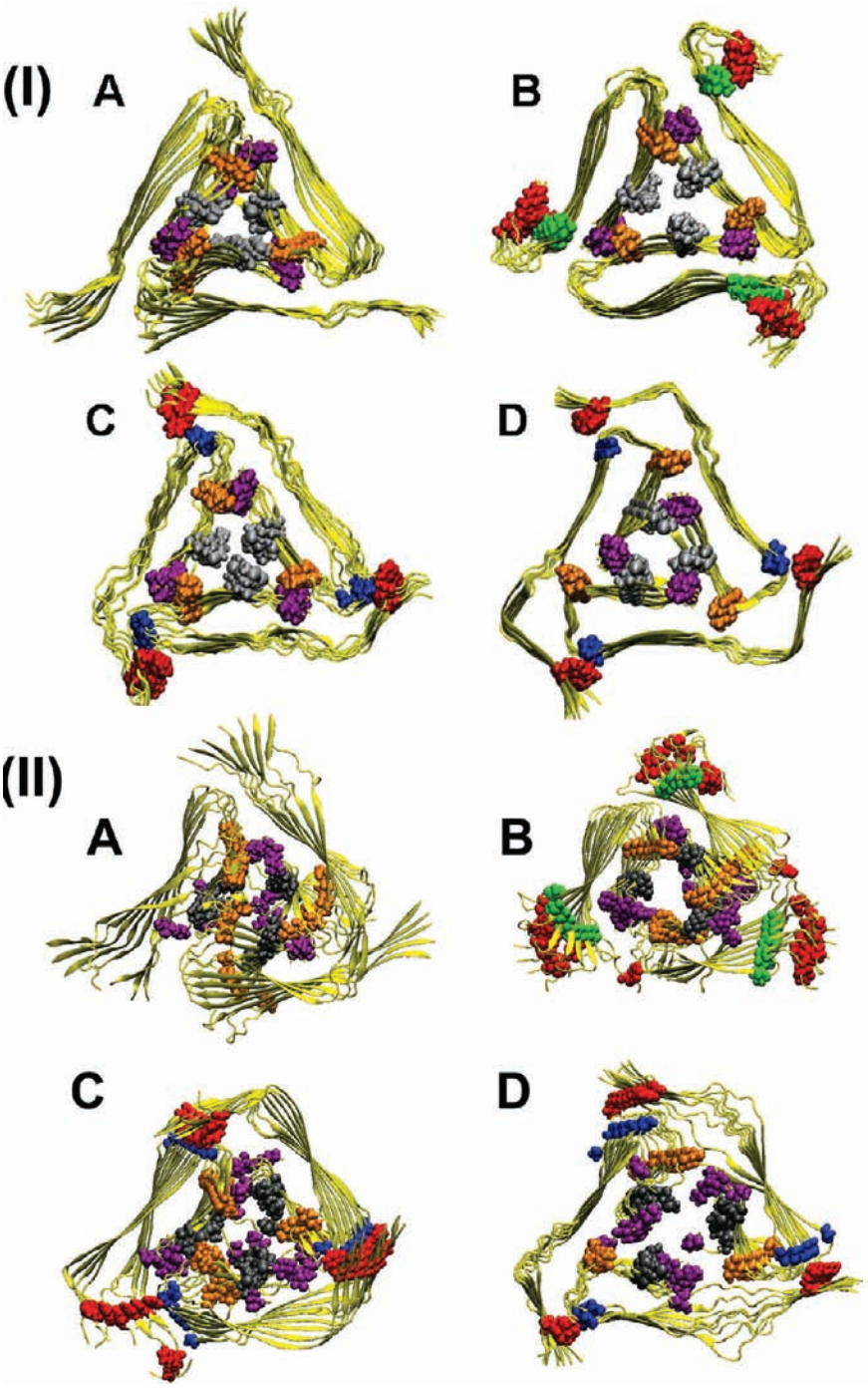

Figure 1. Experiment-based three-fold symmetry conformers before (I) and after (II) simulations of 60 ns. In all four conformers the M35 residues (gray) form the hydrophobic core. Conformers 1, 2, and 3 are based on Tycko's model. The N-termini (residues D1−S8) were linked to the C-termini (residues G9−V40). Conformer 4 is based on Lührs's model. The N-termini (residues D1−L16) were linked to C-termini (residues L17−V40). Residues I41 and A42 were removed from the PDB 2BEG file. In conformers based on Tycko's model, the I31 (orange) and V39 (purple) form contacts between different cross-β units, while in the conformer based on Lührs's model, the M35 and V39 form contacts between the different cross-β units. (A) Conformer 1: The N-termini are flexible and do not interact with any domain in the peptides. (B) Conformer 2: F4 (red) in the N-termini form hydrophobic interactions with V12 (green) in the C-termini. (C) Conformer 3: F4 (red) in the N-termini form hydrophobic interactions with G25 (blue) in the loop regions. (D) Conformer 4: F4 (red) in the N-termini form hydrophobic interactions with G25 (blue) in the loop regions.

three conformers of $A\beta_{1-40}$ (Figure 1A−C), where each conformer consists of 24 monomers: three parallel octamers arranged in a triangular shape. For each monomer, we linked the G9 to the N-terminal fragment peptide (D1−S8). All three conformers exhibit contacts between different cross-β units that are related by the three-fold symmetry (I31−V39 interactions). The three conformers differ in the N-termini (D1−S8) orientations: in conformer 1, the N-termini are flexible and do not interact with any domain of the peptides (Figure 1A). Conformer 2 presents a contact between F4 in the N-terminal and V12 in the C-terminal of each monomer (Figure 1B) and conformer 3 was constructed by forming interactions between F4 in the

dx.doi.org/10.1021/ja1100273 |*J. Am. Chem. Soc.* 2011, 133, 2742–2748

Table 1. Conformational Energy of the Four Constructed Conformers

$A\beta_{1-40}$ conformer	experiment-based model	interactions	conformational energy (kcal/mol)[a]	
1	Tycko[6]	none	−24 977.7 (433.1)	−25 069.1 (387.7)
2	Tycko[6]	F4−V12	−25 340.5 (390.5)	−25 576.3 (310.1)
3	Tycko[6]	F4-G25	−25 156.8 (390.7)	−25 378.3 (415.5)
4	Lührs[7]	F4-G25	−25 176.1 (385.4)	−25 320.2 (397.6)

[a] Conformational energies were computed using the GBMV calculations. The standard deviation values are presented in parentheses. The conformational energies in the fourth and fifth columns are computed for different initial states of conformers.

N-termini of one octamer and G25 in the loops region of a nearby octamer (Figure 1C). To study the polymorphism due to the U-turn shape of the three-fold symmetry model, we constructed one conformer of $A\beta_{1-40}$ (conformer 4, Figure 1D) based on Lührs's model for the $A\beta_{17-42}$ coordinates (PDB: 2BEG).[8] We note that Lührs's model has coordinates for one layer of $A\beta_{17-42}$. We used the third monomer conformation of the $A\beta_{17-42}$ peptide from the $A\beta$ pentamer in the PDB coordinate file and generated three parallel octamers arranged in a triangular shape. Residues I41 and A42 were removed from each monomer, and the L17's of each monomer were linked to the N-terminal fragment peptide (D1−K16). This conformer was also constructed by forming interactions between F4 in the N-termini of one octamer and G25 in the loops region of a nearby octamer, as in conformer 3. However, while all three conformers based on Tycko's model demonstrate I31−V39 interactions between cross-β units in the three-fold symmetry structure, these interactions are not present in the conformer based on Lührs's model. We note that we tested a conformer based on Lührs's model with I31−V39 interactions; however, this conformer exhibits an unstable structure (Figure S1, Supporting Information).

Conformer 1 was constructed using directly the 6-mer (i.e., six layers) coordinates provided by Tycko's laboratory, with two additional layers. For conformer 4, we used the third monomer conformation of the $A\beta_{17-42}$ peptide from the $A\beta$ pentamer in the PDB 2BEG coordinate file, and generated three 8-mer oligomers in a parallel arrangement in the three-fold symmetry structure.

To study the effect of the pH on the structural stability and the populations, we used different protonation states of titratable side chains to simulate the constructed models at different pH values. For pH = 7, only the positively charged residues (Lys and Arg) were protonated.

2.2. Molecular Dynamics (MD) Simulations Procedure. Molecular dynamics simulations of solvated $A\beta_{1-40}$ oligomers were performed in the NPT ensemble using the NAMD program[9] with the CHARMM27 force field.[10,11] The oligomers were explicitly solvated with TIP3P water molecules.[12,13] The Langevin piston method[14−16] with a decay period of 100 fs and a damping time of 50 fs was used to maintain a constant pressure of 1 atm (1 atm = 101.3 kPa). The temperature (300 K) was controlled by Langevin thermostat with a damping coefficient of 10 ps^{-1}.[14] The short-range van der Waals interactions were calculated using the switching function, with a twin range cutoff of 10.0 and 12.0 Å. Long-range electrostatic interactions were calculated using the particle mesh Ewald method with a cutoff of 12.0 Å for all simulations.[17,18] The equations of motion were integrated using the leapfrog integrator with a step of 2 fs.

All initial $A\beta_{1-40}$ oligomers were energy minimized and then solvated in a TIP3P water box with a minimum distance of 10 Å from any edge of the box to any $A\beta$ atom. Any water molecule within 2.5 Å of the $A\beta$ was removed. Counterions (Na^+) were added at random locations to neutralize the $A\beta_{1-40}$ charge.

The solvated systems were energy minimized for 2000 conjugated gradient steps, where the hydrogen bond distances between the β-sheets in $A\beta_{1-40}$ were fixed in the range 2.2−2.5 Å. The counterions and water molecules were allowed to move. The hydrogen atoms were constrained to the equilibrium bond using the SHAKE algorithm.[19] The minimized solvated systems were heated for additional 5000 conjugate gradient steps at 250 K, where all atoms were allowed to move. The systems were then heated from 250 to 300 K for 300 ps and equilibrated at 300 K for 300 ps. All simulations ran for 60 ns, and structures were saved every 10 ps for analysis. These conditions (300 K and 60 ns of time scales) are applied to test the stabilities of all $A\beta_{1-40}$ oligomers.

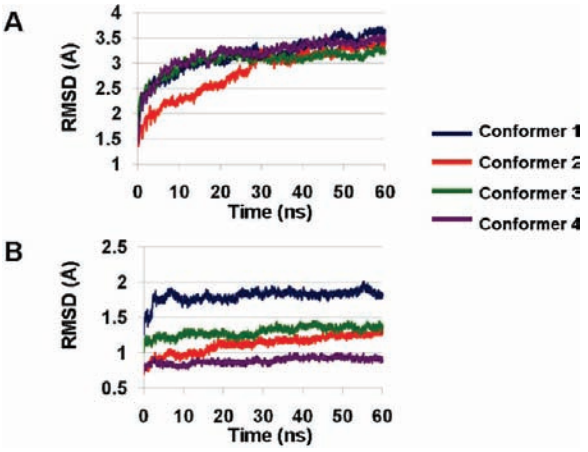

Figure 2. Root-mean-square deviations of conformers based on Tycko's and Lührs's models. The RMSDs are computed separately for the two parts of each of the four conformers: C-terminal (residues 17−40) and U-turn (residues 22−29).

For each conformer a single MD simulation was performed where the systems were heated from 250 to 300 K for 300 ps and equilibrated at 300 K for 300 ps. To test the results obtained from these MD simulations, we ran simulations with different initial conditions for each conformer: the systems were heated from 100 to 200 K for 300 ps and equilibrated at 250 K for 300 ps. Those different initial conditions still lead to the same simulation results. M35−M35 distance values demonstrate similar distributions (Figure S2, Supporting Information), and the conformational energies (Table 1) illustrate that the stabilities of the four conformers follow the same trend.

2.3. Generalized Born Method with Molecular Volume (GBMV). In the GBMV calculations,[20,21] the dielectric constant of water was set to 80. The hydrophobic solvent-accessible surface area term factor was set to 0.00592 kcal/mol·$Å^2$. Each conformer was minimized using 1000 cycles, and the conformational energy was evaluated by grid-based GBMV. The minimization does not change the conformations of each conformer; it only relaxes the local geometries due to thermal fluctuation which occurred during the MD simulations.

2.4. Analysis Details. The core cavity is defined by the three averaged values of Cε of M35−Cε of M35 distances along the fibril cavity. The relative conformational stabilities of the oligomers were measured by root-mean-squared deviation (RMSD) of the C-terminal region (residues L17−V40), the N-terminal region (residues A2−Q15), and the U-turn region (residues E22−G29) with respect to the initial minimized structure throughout the simulations. We followed the change in the D23−K28 distance: the averaged distance between Cγ of D23 and N

dx.doi.org/10.1021/ja1100273 |J. Am. Chem. Soc. 2011, 133, 2742–2748

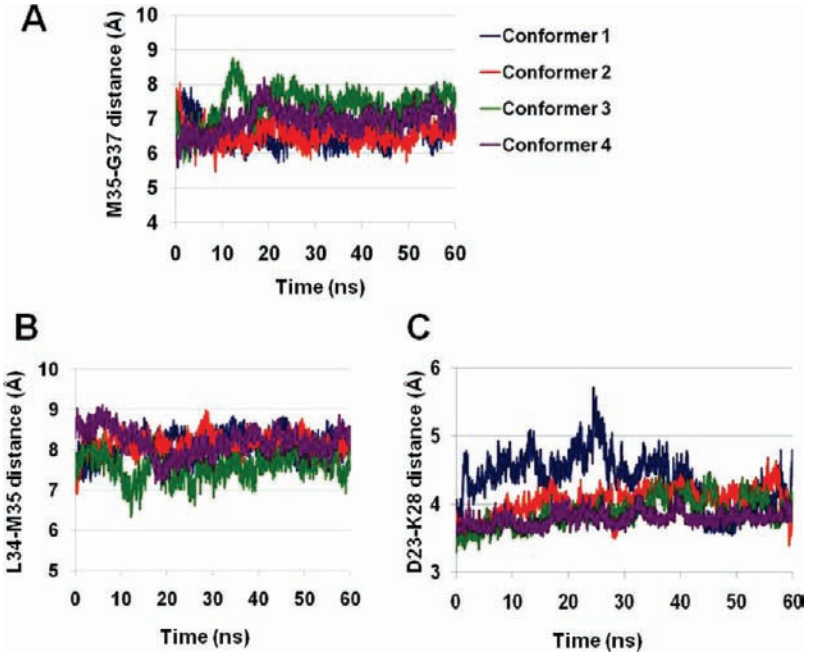

Figure 3. (A) Averaged M35−G37 distances within the peptide for all four conformers. (B) Averaged L34−M35 distances within the peptide for all four conformers. (C) Averaged distance between Cγ of Asp23 and N side chain of Lys for all four conformers.

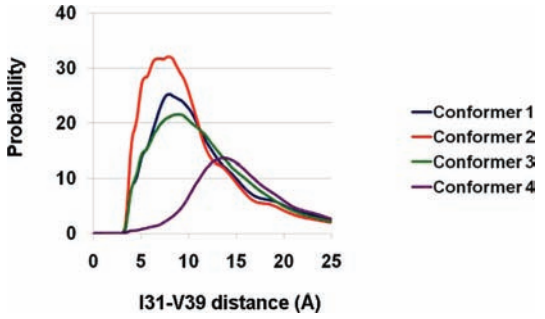

Figure 4. Distribution of the I31−V39 distance for all four conformers.

side chain of K28 in the same peptide, and the averaged distance of the two C═O bonds of D23 to the N atom in K28 in the same peptide.

The structural stability of the constructed conformers was tested by following the change in the distances: M35−G37 and L34−M35 distances between the methyl carbon of M35 and the backbone nitrogen sites of G37 and L34; Cε of M35−Cε of M35 along the fibril axis, Cε of M35−amine group of G37 within the same peptide, amine group of L34−Cε of M35 also within the same peptide, and Cβ of I31−Cβ of V39 between cross-β units in the three-fold symmetry structure. All distances were calculated for each of the eight layers separately and then averaged. Finally, the probabilities of the distances F4−V12, M35−M35 along the fibril cavity and I31−V39 between cross-β units in the three-fold symmetry structure were computed from average distances of all atoms.

3. RESULTS

3.1. Conformational Stability of Aβ_{1-40} Oligomers: Polymorphic N-Terminal Arrangements. In order to compare potential oligomers, we constructed four conformers of the three-fold symmetry model and generated 500 conformations for each arrangement by MD simulations. Our simulations indicated that all four conformers are structurally stable, suggesting that they could

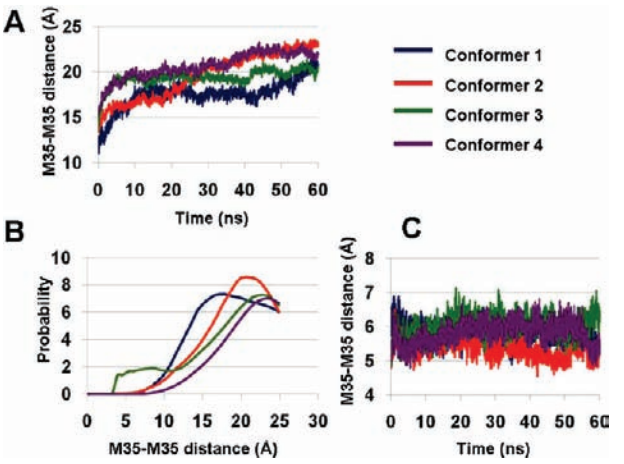

Figure 5. (A) Averaged M35−M35 distances in the cavity region along the simulations for all four conformers. (B) Distribution of the M35−M35 distances for all four conformers indicates a cavity along the fibril axis. (C) Averaged M35−M35 distances along the fibril axis for all four conformers during the time of simulation.

exist under physiological conditions: both the C-termini and U-turn RMSDs are low (Figure 2).

Focusing on stability and populations, we test various distances and compared the constraints observed from ssNMR[7] for the experiment-based model with the averaged distances in our conformers. The reported constraints are the intra-peptide M35−G37 and L34−M35 and the salt-bridge D23−K28 distances. All the averaged distances in the constructed conformers exhibit a good agreement with the reported experimental constraints (Figure 3 and Figure S3, Supporting Information). The methyl carbon of M35 fluctuates along the simulations; therefore, when the methyl carbon points to G37 the M35−G37 distance decreases, and when it points to L34 the L34−M35

dx.doi.org/10.1021/ja1100273 |J. Am. Chem. Soc. 2011, 133, 2742–2748

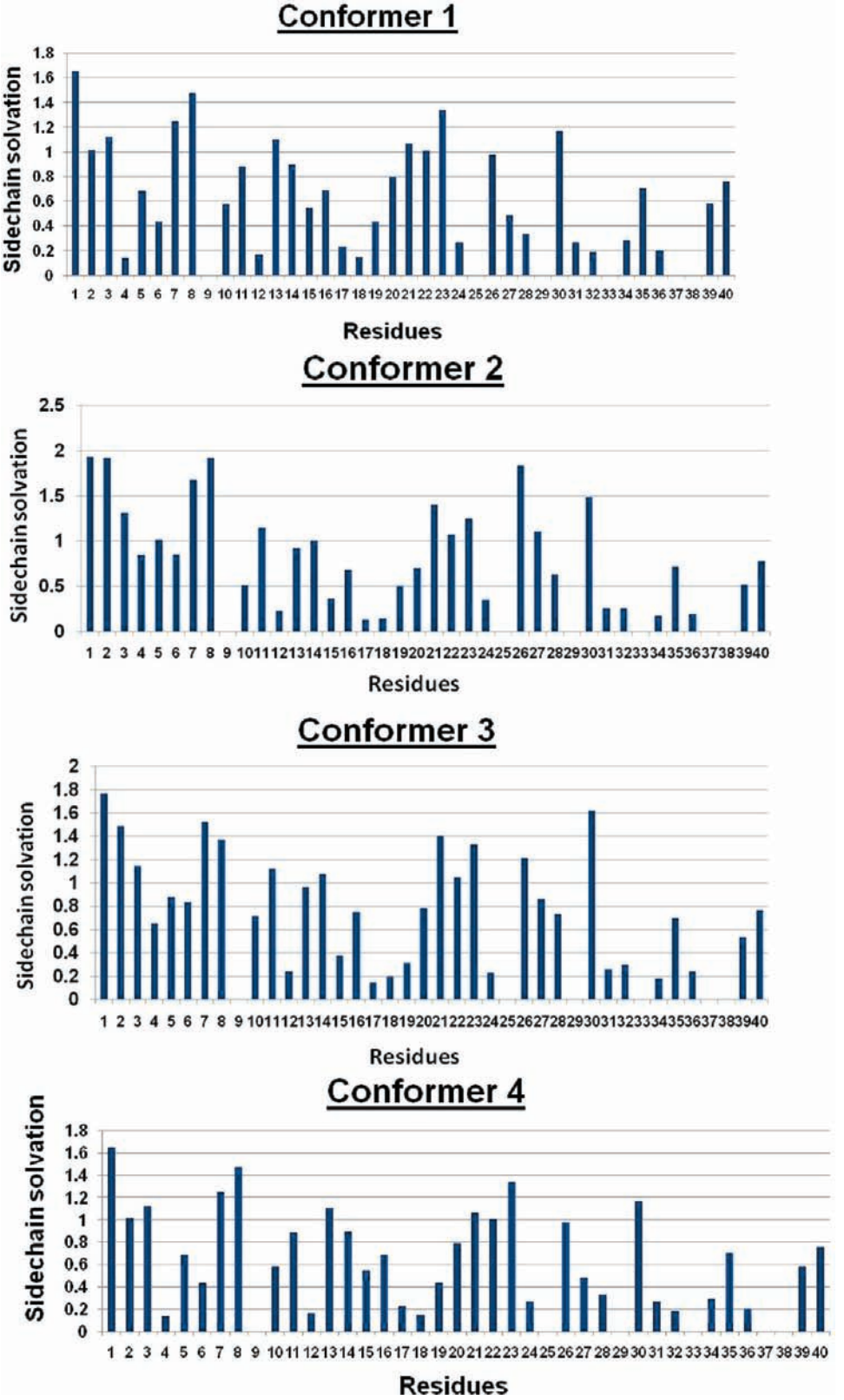

Figure 6. Average water molecules around each side-chain Cβ carbon within 4 Å. Glycines has no side-chain Cβ carbon, which results in zero value in the plots. In all conformers, Met35 has higher solvation exposure than L34 and V36, indicating the existence of water in the hollow hydrophobic core.

decreases. For example, as seen in Figure 3, the M35−G37 distance for conformer 3 at around 10 ns increases to ∼8.5 Å, while around this time scale the L34−M35 distance is ∼6.5 Å. At 17 ns, the M35−G37 distance decreases to ∼6.5 Å, whereas the L34−M35 distance is ∼8.5 Å. Finally, the I31−V39 contacts between cross-β units that are related by the three-fold symmetry

dx.doi.org/10.1021/ja1100273 |*J. Am. Chem. Soc.* 2011, 133, 2742–2748

illustrate a ~6−7 Å distance for all conformers based on Tycko's model (in agreement with experiment) and of ~13 Å for Lührs's model (Figure 4). In Lührs's model the loop region shape differs from that in Tycko's, leading to the larger distances between the I31−V39 contacts. The proximity of the V39−I31 residues may contribute to the stabilization of the cavity along the fibril axis, as illustrated in the next section.

3.2. The Triangular Fibril Has a Stable Cavity along the Fibril Axis. From a top view along the fibril axis of the experiment-based model (Figure 4 in ref 7), the interactions between the three M35 in each layer exhibit a hydrophobic cluster in the interior cross section without a cavity. However, all four constructed conformers reveal a stable cavity along the fibril axis. Figure 5A illustrates that the averaged M35−M35 distances along the simulations increased and stabilized for each conformer. The M35−M35 distance distribution across the fibril cavity shows high cavity probability, with ~16, ~20, ~21, and ~23 Å respectively for conformers 1−4 (Figure 5B). In addition, conformer 3 presents a smaller (~7 Å) cavity for a short duration, due to the initial conformation used in simulation. The averaged M35−M35 distances for a cavity across the fibril axis in our conformers are much larger than 7 Å. However, in our conformers the averaged M35−M35 distances along the fibril axis are in the range of 5−7 Å (Figure 5C). Therefore, our interpretation of the ssNMR observation suggests that the 5−7 Å averaged M35−M35 distances are due to M35−M35 distances along the fibril axis and not across the cavity.

It is of interest to examine whether water molecules exist in the hollow hydrophobic core in all four conformers studied here. Therefore, we computed the averaged solvation of the side chains of all residues in each conformer. Figure 6 demonstrates that Met35 has higher solvation exposure than L34 and V36, indicating the presence of water in the hollow hydrophobic core. The methyl carbons of the M35 residues point into the hollow hydrophobic core; therefore, the side chains of the M35 are relatively 4 times more solvated than the side chains of L34 and V36. Other side chains of residues in the hollow core domain (I31−L34 and V36−A40) do not point to the hollow core, and thus do not exhibit large solvation.

Tycko's group also presented paramagnetic relaxation enhancement data for the three-fold-symmetric Aβ_{40} structure, indicating that M35 is less influenced by Cu^{2+}-EDTA than I32. In another paramagnetic relaxation enhancement study, Wickramasinghe et al.[22] found that I31 and I32 have relaxation rate enhancement similar to that for a two-fold symmetry fibril. Regardless of whether the paramagnetic relaxation enhancement can be explained by M35 being more buried than I31/I32, M35 side-chain methyl carbons may not be accessible to Cu^{2+}-EDTA in solution. We examined if the cavity size allows free access of Cu^{2+}-EDTA into the interior. As can be seen in Figure 7, entry of Cu^{2+}-EDTA into the cavity clashes with the Connolly surface. Thus, Cu^{2+}-EDTA needs complementary force to allow its binding with the fibril cavity. Such a scenario rarely happens between Cu^{2+}-EDTA and any protein, as there is no EDTA−protein complex in the entire protein structural database (PBD). Hence, our results indicated that the cavity size found in our study still does not allow close encounter of Cu^{2+}-EDTA and M35, I31, and I32.

3.3. Polymorphic Aβ_{1-40} Oligomers: Hydrophobic Interactions of the N-Terminal with the C-Terminal and U-Turn. For the complex kinetics of amyloid formation, the four constructed conformers are likely to represent only a very small percentage of the ensemble. Nevertheless, the carefully selected

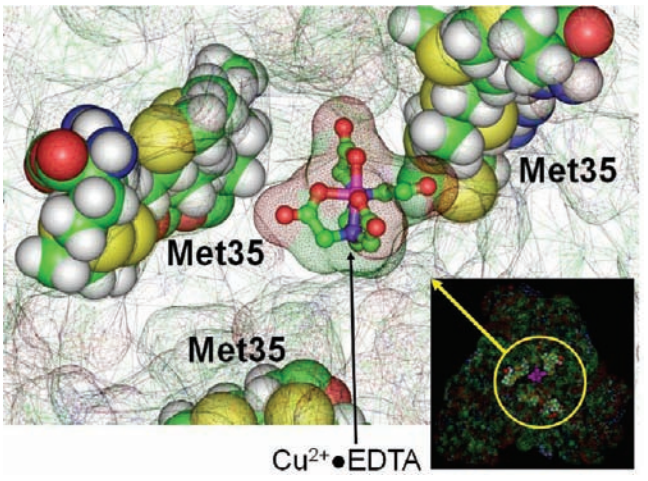

Figure 7. The fibril cavity size is not large enough to allow free access of Cu^{2+}-EDTA. M35 is represented by balls with the sulfur in yellow. The bottom right corner illustrates the overall Connolly surface of the three-fold symmetry conformer 2, with the Cu^{2+}-EDTA as a ball sitting in the center. The enlarged figure shows the clash of the Connolly surfaces of Cu^{2+}-EDTA and conformer 2. Cu^{2+}-EDTA is represented by ball-and-stick, with oxygen in red, nitrogen in blue, and Cu^{2+} in magenta.

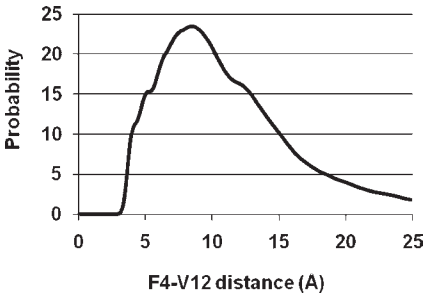

Figure 8. Distribution of the F4−V12 distance for conformer 2.

conformers sample the most likely organizations. On the basis of Monte Carlo simulations with the energy landscape computed with GBMV, we estimated the relative stabilities of all constructed conformers. Conformer 1, which is based on Tycko's model and exhibits nonhydrophobic interactions between the N-termini and other regions in the Aβ peptides, is energetically less stable compared to the others (Table 1). However, conformer 2 (also based on Tycko's model) forms strong hydrophobic interactions between the C- and the N-termini (~7 Å between F4 and V12) within each monomer (Figure 8) and is the most stable. So far, it was believed that the disordered N-terminal segment is not involved in fibril formation. However, here we show that the intramolecular interactions between the flexible N-terminal and the C-terminal within each peptide in the triangular fibril structure stabilize the conformer. In addition, as seen in conformer 3, intermolecular hydrophobic interactions (F4−G29) between the flexible N-terminal of one Aβ peptide and the loop region of another demonstrate increased stability compared with conformer 1. Consequently, we suggest that the N-terminal stabilizes the fibril and thus plays a role in fibril formation. Finally, loop flexibility allows slightly different loop types which contribute to polymorphic amyloid morphologies. Herein, we constructed the triangular Aβ with two experiment-based coordinates which differ in the loop region: conformer 3

dx.doi.org/10.1021/ja1100273 |J. Am. Chem. Soc. 2011, 133, 2742–2748

based on Tycko's file and conformer 4 based on Lührs's PDB file. The similar energies of conformers 3 and 4 (Table 1) indicate that the triangular $A\beta_{40}$ structures based on the two different U-turn shapes have similar stabilities and consequently further confirm a likely polymorphic scenario in amyloid formation.[23]

4. DISCUSSION AND CONCLUSIONS

The hydrophobic cavity in $A\beta_{1-40}/A\beta_{1-42}$ amyloid structures was observed in previous studies.[6,24−27] Water molecules travel along the hydrophobic cavity of these structures to form hydrogen bond interactions with residues in the cavity domain. This stabilizes the cavity and allows optimization of the intermolecular sheet−sheet packing. The role of the hydrated hydrophobic cavity in amyloids is still controversial, because the mechanism of the amyloid toxicity is not yet clear. Herein, we demonstrate a stable cavity in the three-fold symmetry experiment-based model for $A\beta_{1-40}$ with dimensions in a range of 16−23 Å for the constructed models. Recently, Zheng et al.[24] reported a cavity also in the three-fold symmetry experiment-based model for $A\beta_{9-40}$ with similar dimension in the interior cross section (∼20.4 Å).

Our study leads to an important conclusion: the triangular structure studied here exhibits a cavity along the fibril axis and is stabilized by I31−V39 contacts between cross-β units and N-terminal interactions with the U-turn region. Recently, a cryoEM density map of two-fold symmetry $A\beta_{1-42}$ fibrils also led to a model which presented a hollow core and N-terminal−turn interactions.[25] Both the $A\beta_{1-42}$ two-fold and the triangular $A\beta_{1-40}$ three-fold symmetry conformers share these features and are stabilized by across-the-fibril-axis N-terminal−U-turn interactions. However, while the C-terminal faces inside the core in the three-fold $A\beta_{1-40}$ fibril, in the $A\beta_{1-42}$ fibril the N-terminal is more likely to face inside the hollow core, as illustrated by Miller et al.[28] These common features argue for consideration in AD drug design.

Finally, it should be noted here that the N-terminal may and probably does play a role in aggregation. However, simulation[29] and experimental[30] studies suggest that even if the N-terminal participates in aggregation, it does not determine the aggregation interface.

■ ASSOCIATED CONTENT

Supporting Information. Complete ref 10; Figures S1−S3. This material is available free of charge via the Internet at http://pubs.acs.org.

■ AUTHOR INFORMATION

Corresponding Author
mabuyong@mail.nih.gov; ruthnu@helix.nih.gov

■ ACKNOWLEDGMENT

We thank Rob Tycko for providing the atomic coordinates of the model obtained in his laboratory. All simulations had been performed using the high-performance computational facilities of the Biowulf PC/Linux cluster at the National Institutes of Health, Bethesda, MD (http://biowulf.nih.gov). This project has been funded in whole or in part with Federal funds from the National Cancer Institute, National Institutes of Health, under contract no. HHSN261200800001E. This research was supported in part by the Intramural Research Program of the NIH, National Cancer Institute, Center for Cancer Research.

■ REFERENCES

(1) Fraser, P. E.; Levesque, L.; McLachlan, D. R. *Clin. Biochem.* **1993**, *26*, 339.
(2) Naslund, J.; Schierhorn, A.; Hellman, U.; Lannfelt, L.; Roses, A. D.; Tjernberg, L. O.; Silberring, J.; Gandy, S. E.; Winblad, B.; Greengard, P.; Nordstedt, C; Terenius, L. *Proc. Natl. Acad. Sci. U.S.A.* **1994**, *91*, 8378.
(3) Mori, H.; Takio, K.; Ogawara, M.; Selkoe, D. J. *J. Biol. Chem.* **1992**, *267*, 17082.
(4) Walsh, D. M.; Hartley, D. M.; Kusumoto, Y.; Fezoui, Y.; Condron, M. M.; Lomakin, A.; Benedek, G. B.; Selkoe, D. J.; Teplow, D. B. *J. Biol. Chem.* **1999**, *274*, 25945.
(5) Morgan, C.; Colombres, M.; Nunez, M. T.; Inestrosa, N. C. *Prog. Neurobiol.* **2004**, *74*, 323.
(6) Petkova, A. T.; Yau, W. M.; Tycko, R. *Biochemistry* **2006**, *45*, 498.
(7) Paravastu, A. K.; Leapman, R. D.; Yau, W. M.; Tycko, R. *Proc. Natl. Acad. Sci. U.S.A.* **2008**, *105*, 18349.
(8) Lührs, T.; Ritter, C.; Adrian, M.; Riek-Loher, D.; Bohrmann, B.; Dobeli, H.; Schubert, D.; Riek, R. *Proc. Natl. Acad. Sci. U.S.A.* **2005**, *102*, 17342.
(9) Kale, L.; Skeel, R.; Bhandarkar, M.; Brunner, R.; Gursoy, A.; Krawetz, N.; Phillips, J.; Shinozaki, A.; Varadarajan, K.; Schulten, K. *J. Comput. Phys.* **1999**, *151*, 283.
(10) MacKerell, A. D.; et al. *J. Phys. Chem. B* **1998**, *102*, 3586.
(11) Brooks, B. R.; Bruccoleri, R. E.; Olafson, B. D.; States, D. J.; Swaminathan, S.; Karplus, M. *J. Comput. Chem.* **1983**, *4*, 187.
(12) Mahoney, M. W.; Jorgensen, W. L. *J. Chem. Phys.* **2000**, *112*, 8910.
(13) Jorgensen, W. L.; Chandrasekhar, J.; Madura, J. D.; Impey, R. W.; Klein, M. L. *J. Chem. Phys.* **1983**, *79*, 926.
(14) Kale, L.; Skeel, R.; Bhandarkar, M.; Brunner, R.; Gursoy, A.; Krawetz, N.; Phillips, J.; Shinozaki, A.; Varadarajan, K.; Schulten, K. *J. Comput. Phys.* **1999**, *151*, 283.
(15) Martyna, G. J.; Tobias, D. J.; Klein, M. L. *J. Chem. Phys.* **1994**, *101*, 4177.
(16) Feller, S. E.; Zhang, Y. H.; Pastor, R. W.; Brooks, B. R. *J. Chem. Phys.* **1995**, *103*, 4613.
(17) Darden, T.; York, D.; Pedersen, L. *J. Chem. Phys.* **1993**, *98*, 10089.
(18) Essmann, U.; Perera, L.; Berkowitz, M. L.; Darden, T.; Lee, H.; Pedersen, L. G. *J. Chem. Phys.* **1995**, *103*, 8577.
(19) Ryckaert, J. P.; Ciccotti, G.; Berendsen, H. J. C. *J. Comput. Phys.* **1977**, *23*, 327.
(20) Lee, M. S.; Salsbury, F. R.; Brooks, C. L. *J. Chem. Phys.* **2002**, *116*, 10606.
(21) Lee, M. S.; Feig, M.; Salsbury, F. R.; Brooks, C. L. *J. Comput. Chem.* **2003**, *24*, 1348.
(22) Wickramasinghe, N. P.; Parthasarathy, S.; Jones, C. R.; Bhardwaj, C.; Long, F.; Kotecha, M.; Mehboob, S.; Fung, L. W.; Past, J.; Samoson, A.; Ishii, Y. *Nat. Methods* **2009**, *6*, 215.
(23) Miller, Y.; Ma, B.; Nussinov, R. *Biophys. J.* **2009**, *97*, 1168.
(24) Zheng, J.; Yu, X.; Wang, J.; Yang, J.-C.; Wang, Q. *J. Phys. Chem. B* **2010**, *114*, 463.
(25) Zhang, R.; Hu, X.; Khant, H.; Ludtke, S. J.; Chiu, W.; Schmid, M. F.; Frieden, C.; Lee, J. M. *Proc. Natl. Acad. Sci. U.S.A.* **2009**, *106*, 4653.
(26) Sato, T.; Kienlen-Campard, P.; Ahmed, M.; Liu, W.; Li, H.; Elliott, J. I.; Aimoto, S.; Constantinescu, S. N.; Octave, J. N.; Smith, S. O. *Biochemistry* **2006**, *45*, 5503.
(27) Zheng, J.; Jang, H.; Ma, B.; Tsai, C. J.; Nussinov, R. *Biophys. J.* **2007**, *93*, 3046.
(28) Miller, Y.; Ma, B.; Tsai, C. J.; Nussinov, R. *Proc. Natl. Acad. Sci. U.S.A.* **2010**, *107*, 14128.
(29) Takeda, T.; Klimov, D. K. *J. Phys. Chem. B* **2009**, *113*, 6692.
(30) Bitan, G.; Vollers, S. S.; Teplow, D. B. *J. Biol. Chem.* **2003**, *278*, 34882.